APPLIED PHYSICS

Propagation and attenuation of mechanical signals in ultrasoft 2D solids

Jan Maarten van Doorn[1], Ruben Higler[1], Ronald Wegh[1], Remco Fokkink[1], Alessio Zaccone[2], Joris Sprakel[1], Jasper van der Gucht[1]*

The propagation of elastic waves in soft materials plays a crucial role in the spatiotemporal transmission of mechanical signals, e.g., in biological mechanotransduction or in the failure of marginal solids. At high Reynolds numbers $Re \gg 1$, inertia dominates and wave propagation is readily observed. However, mechanical cues in soft and biological materials often occur at low *Re*, where waves are overdamped. Overdamped waves are not only difficult to observe experimentally, also theoretically their description remains incomplete. Here, we present direct measurements of the propagation and attenuation of mechanical signals in colloidal soft solids, induced by an optical trap. We derive an analytical theory for low *Re* wave propagation and damping, which is in excellent agreement with the experiments. Our results present both a previously unexplored method to characterize damped waves in soft solids and a theoretical framework showing how localized mechanical signals can provoke a remote and delayed response.

INTRODUCTION

The propagation of elastic waves in soft materials plays a crucial role in the spatiotemporal transmission of mechanical signals, e.g., in biological mechanotransduction (*1*, *2*) or in the failure of marginal solids (*3*–*6*). At high Reynolds numbers $Re \gg 1$, inertia dominates and wave propagation can be readily observed (*7*–*9*). However, mechanical cues in soft and biological materials often occur at low *Re* (*10*), playing a key role in their spatiotemporal response to mechanical perturbations (*11*, *12*). For example, in marginally stable systems, such as jammed packings or fiber networks, a stress at the right position can cause total loss of rigidity (*3*–*6*). In living cells, the propagation of mechanical signals through soft structures is crucial in mechanotransduction (*1*, *2*) and controls, for example, cell differentiation (*13*). Also, in soft robotics, sensing and control require the transmission of mechanical signals over a distance (*14*).

Localized mechanical signals can spread in space and time by propagation of elastic waves (*7*–*9*). This wave propagation is intimately linked to the mechanical properties of the medium (*15*). In very soft materials, the transmission of mechanical signals poses challenges, because their intrinsically dissipative nature leads to energy losses as the wave propagates (*10*, *16*). In particular, at low excitation frequencies, corresponding to low Reynolds numbers, viscous attenuation of the wave signal is strong, and its detection is challenging. Moreover, in ultrasoft solids, the relative amplitudes of thermal fluctuations are large, thus further obscuring robust wave propagation and their detection in experiments.

In this Letter, we show how Fourier filtering can reveal even very weak and strongly damped elastic waves at extremely low Reynolds numbers, $Re \sim 10^{-6}$, in ultrasoft solids formed from crystals and glasses of colloids in two dimensions. We create a localized oscillatory perturbation within these solids with an optical tweezer and use video microscopy and frequency domain filtering to quantify the spatiotemporal strain response. On the basis of an overdamped equation of motion, which is in excellent quantitative agreement with our experimental results, this enables a full characterization of low *Re* wave propagation and attenuation in ultrasoft solids. Moreover, we show how the analysis of these waves can be used to obtain the linear mechanical moduli of very weak elastic solids.

RESULTS

We prepare two-dimensional (2D) colloidal crystals by sedimenting monodisperse silica particles with radius $a = 3.04$ μm suspended in an aqueous buffer at pH 8.4 and an ionic strength of 10 mM, giving a Debye screening length $\kappa^{-1} \approx 3$ nm $\ll a$. This short-ranged electrostatic repulsion yields dense 2D crystals with long-ranged hexagonal order at a packing fraction of 0.84 (Fig. 1A and section S1.1).

To create a propagating mechanical wave, we trap a single particle of the crystal in an optical trap and force it into an in-plane oscillatory motion with an amplitude $A_0 = 2.5$ μm (Fig. 2A). We vary the frequency ω of this motion between 0.05 and 10 rad/s, corresponding to Reynolds numbers between $4 \cdot 10^{-7}$ and $8 \cdot 10^{-5}$ (*17*), and confirm that this mechanical excitation is well within the linear regime (section S2).

Note that the self-diffusion time of particles in the crystal, $\tau = a^2/4D \approx 100$ s, so that the Deborah number $De = \omega\tau$ is larger than 1 in all our experiments (section S3), implying that the material can be considered a viscoelastic solid.

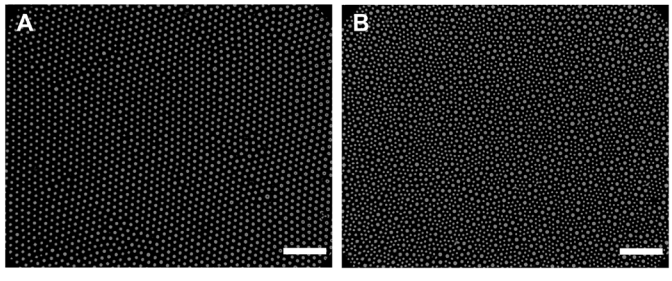

Fig. 1. Structure of colloidal samples. Bright-field microscopy images of (**A**) 2D colloidal crystal and (**B**) 2D colloidal glass of silica particles used in the tweezing experiments. Scale bars, 40 μm.

[1]Physical Chemistry and Soft Matter, Wageningen University and Research, Stippeneng 4, 6708 WE Wageningen, the Netherlands. [2]Department of Chemical Engineering and Biotechnology, University of Cambridge, Cambridge CB3 0AS, UK.
*Corresponding author. Email: jasper.vandergucht@wur.nl

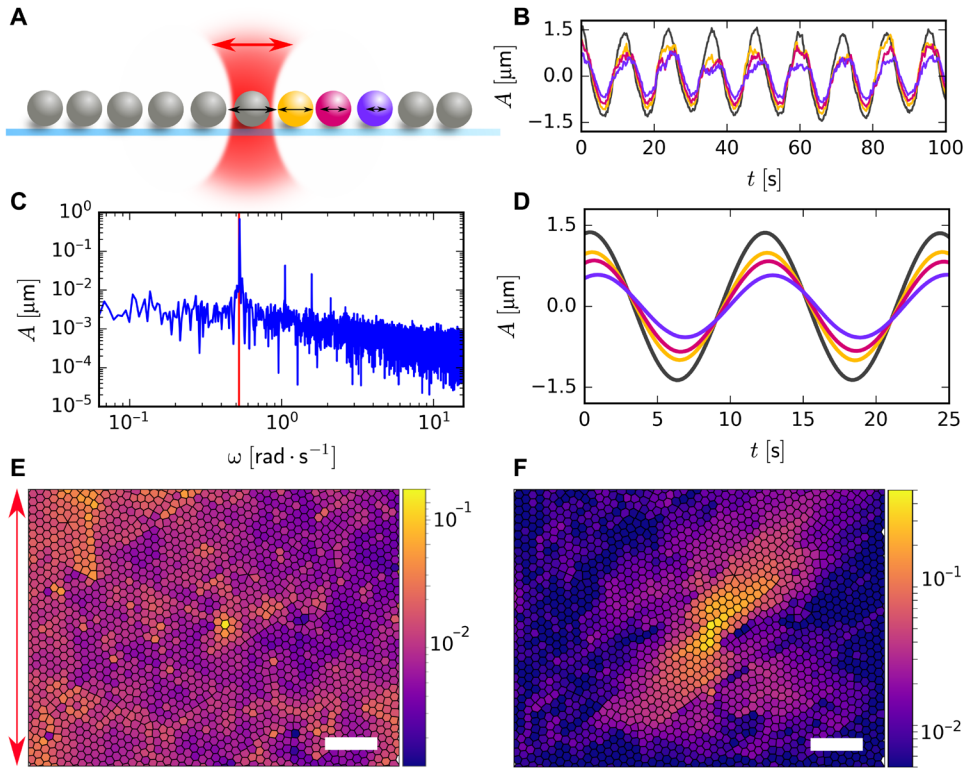

Fig. 2. Generation and detection of mechanical waves. (**A**) Schematic overview of our experiment. (**B**) Raw experimental particle trajectories in the direction of the driven particle (gray). Colors correspond to the particles in (A). (**C**) Amplitude spectrum of the driven particle. The red line corresponds to the driving frequency. (**D**) Trajectories of (B) after Fourier filtering at the driving frequency. (**E**) Unfiltered root mean square displacement and (**F**) Fourier-filtered amplitude map of particles in a crystal excited at ω = 3.1 rad/s; the color scale in (E) and (F) represents the amplitude in micrometers. Scale bars, 40 μm. The red arrow indicates the oscillation direction of the probe particle.

The oscillating particle creates a mechanical wave that propagates through the surrounding material. This sets up a net ballistic displacement of the particles adjacent to the oscillating bead. However, the signal of interest is convolved with the inherent Brownian motion of these microscopic colloids. In particular, far away from the trapped colloid, where the elastic signal is attenuated, it may drown in the Brownian noise (Fig. 2, B and E). Upon filtering the positional trajectory of each particle in the frequency domain at the driving frequency (Fig. 2C), even small displacements due to the propagating wave become apparent (Fig. 2D). To ensure statistical reliability of these data, we set up a real-time distributed particle tracking algorithm that allows us to collect data during 20,000 to 35,000 frames, which is equivalent to 50 to 500 oscillation cycles. While the unfiltered mean square displacement of the particles shows no apparent signature of the perturbation, except at the forced particle (Fig. 2E), the Fourier-filtered amplitude map shows a propagating mechanical wave with an amplitude that decays steeply with increasing distance from the trapped bead (Fig. 2F) and a phase shift that gradually increases with distance (Fig. 2D).

To explain these results, we assume that the colloidal crystal can be treated as a 2D continuous elastic material. We write an equation of motion for the displacement field $\vec{\mathbf{u}}$ in the solid (*18*) to which we add a dissipative term to account for the damping fluid and an oscillating point force, $\vec{\mathbf{f}}(t) = \vec{\mathbf{f}}_0 \cdot e^{i\omega t}$, that represents the perturbation

$$\rho \frac{\partial^2 \vec{\mathbf{u}}}{\partial t^2} + \gamma \frac{\partial \vec{\mathbf{u}}}{\partial t} = \vec{\mathbf{f}}(t)\,\delta(\vec{\mathbf{r}}) + \frac{E}{2(1+\nu)} \vec{\nabla}^2 \vec{\mathbf{u}} + \frac{E}{2(1-\nu)} \vec{\nabla}(\vec{\nabla} \cdot \vec{\mathbf{u}}) \quad (1)$$

Here, the first term describes the inertial forces with $\rho \approx 10^{-2}\,\mathrm{kg/m^2}$ as the density of the 2D material. The second term represents the viscous damping due to the solvent with γ as the drag coefficient per unit area, which we determine experimentally from the short-time diffusion of particles in the crystal, giving $\gamma = 4.8 \cdot 10^3\,\mathrm{Ns/m^3}$ (section S3). The last two terms correspond to the Navier-Cauchy equation that describes the elastic forces within the 2D solid with E as the 2D elastic modulus and ν as the 2D Poisson ratio.

Because our experiments are performed at low Reynolds number, the inertial term is negligible, resulting in overdamped mechanics. Solving the equation of motion for this case yields the displacement field in the form $\vec{\mathbf{u}} = \boldsymbol{\alpha} \cdot \vec{\mathbf{f}}$, with $\boldsymbol{\alpha}$ as the complex response function tensor, which has principal components $\alpha_\parallel$ and $\alpha_\perp$ that describe the components of the displacement field parallel and perpendicular to the applied force, respectively. In polar coordinates, with r as the distance from the point where the force is applied and θ = 0 corresponding to the direction of the force, this becomes (see section S4 for full details)

$$\alpha_\parallel(r,\theta) = \frac{1-\nu^2}{4\pi E}\left(K_0\left(\frac{r\sqrt{i}}{\zeta}\right) + \lambda^2 K_0\left(\frac{r\lambda\sqrt{i}}{\zeta}\right) + \cos(2\theta)\left[K_2\left(\frac{r\sqrt{i}}{\zeta}\right) - \lambda^2 K_2\left(\frac{r\lambda\sqrt{i}}{\zeta}\right)\right]\right) \quad (2)$$

and

$$\alpha_\perp(r,\theta) = \frac{1-\nu^2}{4\pi E}\sin(2\theta)\left[K_2\left(\frac{r\sqrt{i}}{\zeta}\right) - \lambda^2 K_2\left(\frac{r\lambda\sqrt{i}}{\zeta}\right)\right] \quad (3)$$

where K_0 and K_2 denote the modified Bessel functions of the second kind, $\zeta = (\omega\gamma(1-\nu^2)/E)^{-\frac{1}{2}}$ is a characteristic attenuation length of the displacement amplitude, and $\lambda = \sqrt{2/(1-\nu)}$ is a parameter that depends only on the Poisson ratio and diverges for $\nu \to 1$, which is the maximum Poisson ratio in 2D. The amplitude and the phase of the displacement fields are obtained as the magnitude and the argument, respectively, of the complex response functions.

To compare our experimental results with this prediction, we decompose the measured displacement amplitudes into their parallel and perpendicular components (Fig. 3, A and E). This results in distinct lobed patterns for these two components that can be observed in all our experiments. Our theoretical prediction produces identical patterns that are in excellent agreement, indicating that wave propagation in these colloidal crystals can indeed be described by treating the material as a continuous and isotropic 2D elastic solid (Fig. 3, B and F). We note that, in principle, the mechanical properties of the crystal should depend on the direction with respect to the crystal axes, but apparently, such anisotropy does not play a large role for these soft crystals.

The parallel component of the displacement response propagates preferentially along the excitation axis and shows a distinct asymmetry in the attenuation length along the two primary axes. The perpendicular displacement shows a four-lobed pattern, with maximum displacements at an angle of 45° with respect to the excitation direction. Also, in the phase maps (Fig. 3, C and D), we observe patterns that are in excellent agreement with the theoretical prediction (Fig. 3, G and H).

We can now use our theoretical analysis to interpret the experimental results in terms of the linear elasticity of the solid. For this, we first consider the parallel displacement component in the direction of the excitation, $\theta = 0$. An asymptotic expansion of Eq. 2 for relatively large distances from the perturbation $r > \zeta$ (see section S4) leads to a phase lag in the far field

$$\phi_{\parallel}(r,0) \approx -\frac{\pi}{8} - \frac{r}{\zeta\sqrt{2}} \tag{4}$$

and an amplitude

$$A_{\parallel}(r,0) \sim r^{-1/2} e^{-r/\zeta\sqrt{2}} \tag{5}$$

According to Eq. 4, the phase varies linearly with r along $\theta = 0$, which is indeed what we find experimentally (Fig. 4A). This means that the wave propagates at a constant velocity in the direction of the excitation, with a phase velocity $v_{\parallel} = |\,\omega(d\phi_{\parallel}/dr)^{-1}\,| \approx \omega\zeta\sqrt{2} = \sqrt{2E\omega/\gamma(1-\nu)^2}$. As shown in the inset of Fig. 4A, the phase velocity increases approximately as $v_{\parallel} \sim \sqrt{\omega}$ for low frequencies, which indicates that the elastic modulus and the Poisson ratio do not depend on the frequency in this regime.

The linear elasticity of an isotropic 2D solid is described by two independent mechanical parameters: the elastic modulus and the Poisson ratio. While the modulus only affects the absolute magnitude of the response function and the characteristic length scale ζ, the shape of the spatial pattern is uniquely determined by the Poisson ratio, as expressed by the parameter λ in Eqs. 2 and 3 (section S5). Hence, if the Poisson ratio is independent of the frequency, it should be possible to superimpose the measured displacement data obtained at different frequencies by normalizing the distance r by the characteristic length ζ. We determine ζ for each frequency from the asymptotic behavior at large r in two independent ways, using Eqs. 4 and 5. Normalizing all distances with $\zeta(\omega)$ then indeed leads to a collapse of the data for both the amplitude and phase of the parallel displacement contribution, both in the direction of the excitation ($\theta = 0$) and perpendicular to it ($\theta = \pi/2$) (Fig. 4, B and C). We fit these curves to Eq, 2 using $\lambda = \sqrt{2/(1-\nu)}$ as the only fit parameter, giving a value for the Poisson ratio $\nu = 0.70 \pm 0.07$, comparable to values expected for crystalline solids in two dimensions (*19*, *20*). Using this value of ν, we then obtain the elastic moduli of the colloidal crystal from the decay lengths, giving moduli on the order of $E \approx 10^{-6}$ N/m, both for the phase and amplitude data (Fig. 4D). A similar analysis for the perpendicular displacement components, fitted to Eq. 3 (section S6), gives similar moduli (Fig. 4D). As a final consistency check, we use the measured Young's modulus and Poisson ratio to predict the absolute values of the response functions, which now provide a reasonable quantitative

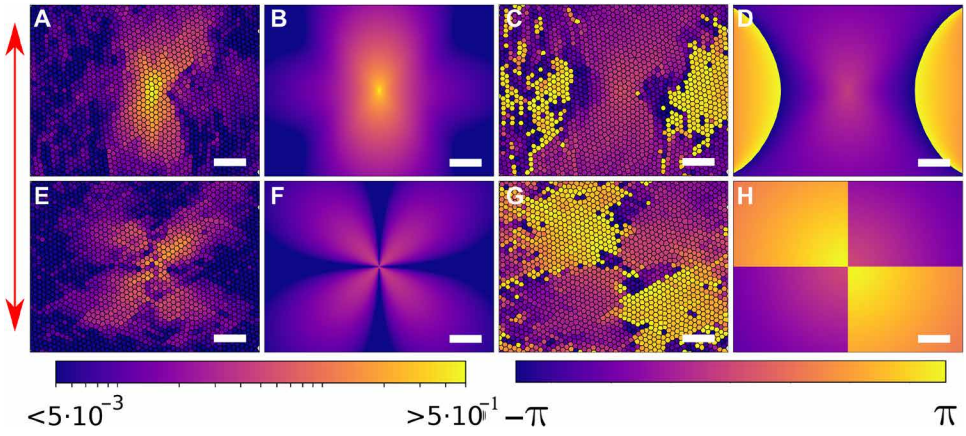

Fig. 3. Comparison of experimental and theoretical wave patterns. (**A**) Experimental amplitude map of the parallel displacement. (**B**) Parallel displacement amplitude predicted by our model. (**C**) Experimental phase shift for the parallel displacement. (**D**) Phase shift of parallel displacement predicted by our model. (**E**) Experimental map of perpendicular displacement. (**F**) Perpendicular displacement amplitude predicted by our model. (**G**) Experimental phase shift for the perpendicular displacement. (**H**) Phase shift of perpendicular displacement predicted by our model. Amplitudes and phases have units micrometers and radians, respectively. Scale bars, 40 μm. The red double-headed arrow indicates the oscillation direction. In all cases, $\omega = 0.52$ rad/s; for the model calculations, $E = 2.5 \cdot 10^{-6}$ N/m and $\nu = 0.7$.

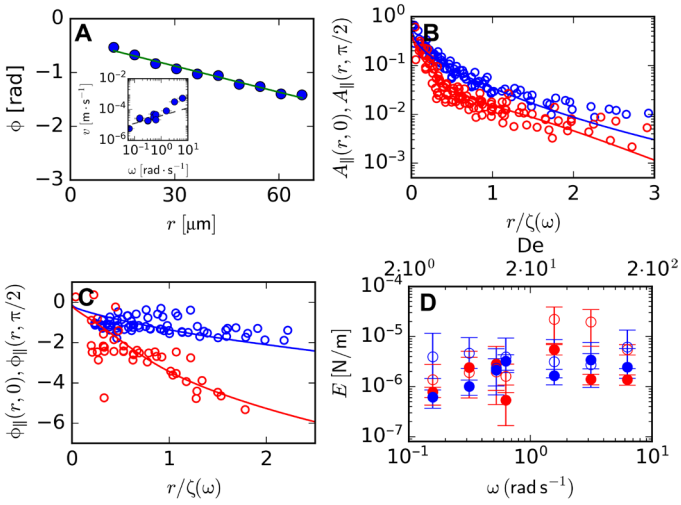

Fig. 4. Analysis of the damped waves. (**A**) Bin-averaged phase of the parallel displacement in the direction of the excitation for $\omega = 0.52$ rad/s. Inset shows the phase velocity versus probed frequency; dashed line depicts slope $\frac{1}{2}$; error bars depict a 95% confidence interval. (**B**) Superposition of parallel displacement amplitude for different frequencies along $\theta = 0$ (blue) and $\theta = \pi/2$ (red) versus normalized distance. (**C**) Superposition of parallel displacement phase for different frequencies along $\theta = 0$ (blue) and $\theta = \pi/2$ (red) versus normalized distance. Lines in (C) and (D) are fits to the theory (with $\nu = 0.7$). (**D**) Elastic modulus as a function of frequency, obtained from the phase (open symbols) and amplitude (filled symbols) of both the parallel (red) and perpendicular (blue) displacement components; error bars depict 95% confidence intervals.

match with the experimental results (Fig. 3, A to H). This highlights that our theoretical description captures the main phenomena in a quantitative fashion.

We may compare the values for E with a simple estimate obtained by approximating the colloidal crystal as a hexagonal lattice of harmonic springs, for which $E = 2k/\sqrt{3}$ with k as the spring constant of a particle pair (*21*). We estimate k by analyzing the thermal bond length fluctuations (section S7) and find $E \approx 1 \cdot 10^{-6}$ N/m in very good agreement with the experimental values. We also validate our results by estimating the modulus in a different way, by analyzing the long-wavelength thermal fluctuations in the crystal (*22*). As shown in section S8, this gives a modulus that is in good agreement with our estimate based on the wave pattern. Our method has the advantage, however, that it can directly probe the frequency dependence of the elastic moduli. Moreover, we obtain a spatial map of the displacement pattern in real space, which allows us to observe deviations from the predicted pattern and to relate these to the local structure (see below).

We note that our method is limited at higher frequencies by the decrease in the attenuation length with increasing frequency. Once the characteristic length ζ becomes of the order of the particle size, discretization effects hinder the accurate determination of the wave propagation. This gives a limiting frequency $\omega_{max} \approx E/\gamma a^2 \approx 20$ rad/s. For frequencies approaching ω_{max}, our estimation of the modulus becomes inaccurate.

Last, to emphasize that our approach is not exclusive to ordered, crystalline solids, we repeat the experiments described above for a disordered colloidal glass that lacks long-ranged order (*23*, *24*). We prepare monolayers of a bidisperse mixture of silica spheres (a = 3.04 and 1.85 μm at a mixing ratio of 1:2.35 by number and a total packing fraction of 0.80) (Fig. 1B). We confirm the absence of structural order from the liquid-like shape of the pair-correlation function and structure factor, while the particle dynamics are strongly arrested and caged as evidenced from their mean square displacement in the absence of external mechanical excitation (section S1.2).

Despite the very different microstructure, we find that the displacement amplitude and phase patterns are very similar to those observed for the crystals (Fig. 5, A to D). The same analysis (Fig. 5, E and F) as for the crystals (using a drag coefficient γ that is a weighted average over the small and large particles, giving $\gamma = 7.5 \cdot 10^2$ Ns/m^3; see section S3) gives a Poisson ratio $\nu = 0.60 \pm 0.15$ and an elastic modulus on the order of $1 \cdot 10^{-7}$ N/m for the glasses ($\log E = -7.0 \pm 0.4$). This is about an order of magnitude lower than for the crystals, which could be due to the slightly lower packing fraction or the softer interaction potential between the small particles (section S7).

From Fig. 5 (A to D), it is also clear that the wave patterns are noisier for the glasses than for the crystals, even though the decay lengths ζ are comparable. The reason for this is not clear, but it might be related to their disordered structure, which is known to lead to inhomogeneous mechanical properties and nonaffine deformation modes (*25*). Further evidence for a relation between wave propagation and microscopic structure can be seen by looking at the displacement patterns in the vicinity of defects in the colloidal crystal. For example, the pattern in Fig. 2F shows an asymmetry between left and right, which can be attributed to the presence of a dislocation just to the right of the probe particle (section S9). We note that this is not yet captured by the theory, which assumes a homogeneous elasticity.

Our results highlight that the observation of highly damped mechanical waves at low *Re* open up the way for mechanical characterization of both ordered and disordered ultraweak solids. Traditionally, microrheology is the method of choice to characterize the viscoelasticity of very weak elastic materials whose moduli are below the detection limit of conventional macroscopic rheometers. In microrheology, the viscoelastic features of the material are extracted from the Brownian fluctuations of tracer particles embedded in the material (passive microrheology) (*26*) or from the response of an actively forced probe particle (active microrheology) (*27*). However, these methods often fail to give the bulk rheological properties, for example, in very heterogeneous samples where the probe particles sample mostly the pores in the material or in cases where the probe particles locally modify the structure of the material. This can be solved by analyzing cross-correlations between particles that are separated by a distance much larger than the characteristic length scale of the material, in microrheology is a field of science so-called two-particle microrheology (*28*). Alternatively, the elastic properties can be obtained by analyzing the long-wavelength thermal vibrational modes of the material using particle tracking techniques, although extracting the frequency-dependent rheological properties is more challenging in this case (*22*). Our method can be seen as a form of active multiparticle microrheology, in which the complete spatial displacement pattern induced by a local perturbation is mapped out. By filtering out the Brownian noise, we obtain experimental access to the frequency-dependent mechanical properties of extremely soft and fragile systems. In principle, the method can also be extended toward the nonlinear deformation regime by increasing the amplitude of the probe oscillation, although the interpretation in terms of nonlinear elastic moduli will obviously be more challenging.

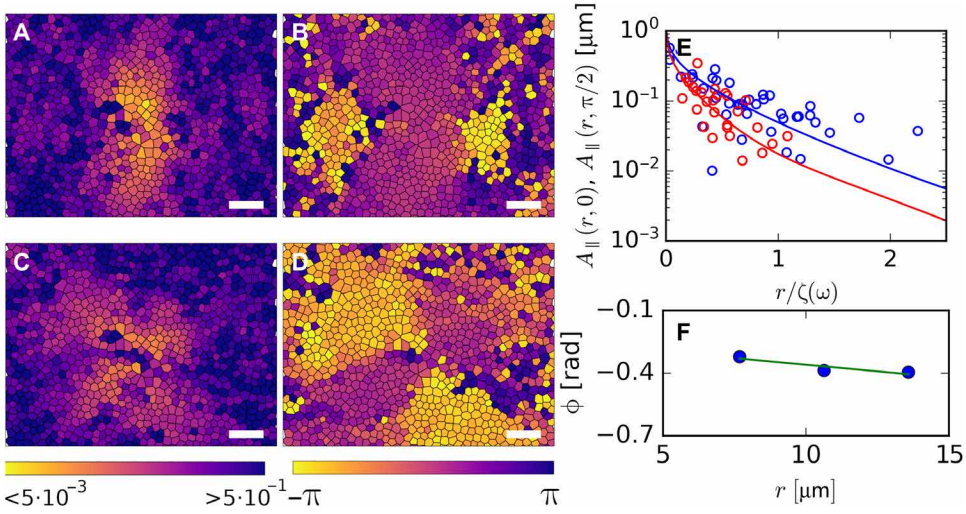

Fig. 5. Waves in colloidal glasses. Experimental maps of (**A**) parallel displacement amplitude, (**B**) parallel displacement phase, (**C**) perpendicular displacement amplitude, and (**D**) perpendicular displacement phase of 2D colloidal glasses excited at $\omega = 0.52$ rad/s. Amplitudes and phases have units micrometers and radians, respectively. Scale bars, 20 μm. (**E**) Superposition of parallel displacement amplitude of colloidal glasses for different frequencies along $\theta = 0$ (blue) and $\theta = \pi/2$ (red) versus normalized distance, together with theoretical prediction ($E = 1.9 \times 10^{-7}$ N/m, $\nu = 0.60$). (**F**) Bin-averaged phase-distance plot to determine phase velocity for $\omega = 0.52$ rad/s in the parallel direction.

DISCUSSION

Here, we have shown how elastic waves can be generated and detected at low *Re* in ultrasoft solids, both ordered and disordered. Moreover, we have proposed an analytical model to describe and interpret the wave attenuation and propagation, which is in excellent quantitative agreement with our experimental results. On the basis of this theory, a measurement of the wave's phase velocity and decay length gives access to the full linear elasticity of the material, giving values in excellent agreement with lattice theory predictions. While our analysis assumes the material to be homogeneous and isotropic, the deviations in the patterns that we observe around defects suggest that wave propagation is affected by heterogeneities in the material. It will be interesting to study these effects in more detail and to generalize, for example, our approach to materials with heterogeneous or anisotropic material properties. In principle, our approach can be extended to probe the mechanics of ultrasoft 3D materials such as biopolymer networks, where the Fourier-filtered elastic displacements can be obtained, e.g., by embedding tracer particles in the material or by using digital image correlation approaches. This could open the way to characterize how localized mechanical signals acting on biological structures give rise to the complex spatiotemporal response that underlies mechanical communication in living organisms and on the role of local structures on the response of marginal networks.

MATERIALS AND METHODS

We prepare 2D colloidal solids by sedimenting monodisperse silica particles (microParticles GmbH) with $a = 304$ μm and $a = 1.85$ μm dispersed in a 10 mM TAPS [tris(hydroxymethyl)methylamino] propanesulfonic acid buffer at pH 8.5. After equilibrating the samples for 48 hours for crystals and 96 hours for glasses, we start an experiment by trapping a particle in the center of the field of view. We make sure that the experiments are performed in a region where there is only a single monolayer, which we check by varying the focus of the microscope. We apply an oscillating force by oscillating the trapped bead with an optical trap at an amplitude of 2.5 μm, using a home-built optical tweezer setup (see section S10). In each experiment, we checked that no particles were pushed out of the layer. The resulting response of the surrounding material is quantified by imaging the colloidal solid with bright-field microscopy and recovering the particle trajectories using established routines (*29*, *30*). We measure at a frame rate of 5 Hz for at least 20,000 frames. We locate particle positions in real time during the experiment by combining existing locating algorithms with a distributed messaging protocol Zero Message Queue (ZMQ). This approach enables to distribute computational load of particle locating over several computers, enabling real-time acquisition.

SUPPLEMENTARY MATERIALS

Supplementary material for this article is available at http://advances.sciencemag.org/cgi/content/full/6/37/eaba6601/DC1

REFERENCES AND NOTES

1. D. E. Ingber, From cellular mechanotransduction to biologically inspired engineering. *Ann. Biomed. Eng.* **38**, 1148–1161 (2010).
2. D. E. Jaalouk, J. Lammerding, Mechanotransduction gone awry. *Nat. Rev. Mol. Cell Biol.* **10**, 63–73 (2009).
3. L. E. Silbert, A. J. Liu, S. R. Nagel, Vibrations and diverging length scales near the unjamming transition. *Phys. Rev. Lett.* **95**, 098301 (2005).
4. L. R. Gómez, A. M. Turner, M. van Hecke, V. Vitelli, Shocks near jamming. *Phys. Rev. Lett.* **108**, 058001 (2012).
5. C. P. Broedersz, X. Mao, T. C. Lubensky, F. C. MacKintosh, Criticality and isostaticity in fibre networks. *Nat. Phys.* **7**, 983–988 (2011).
6. G. Düring, E. Lerner, M. Wyart, Phonon gap and localization lengths in floppy materials. *Soft Matter* **9**, 146–154 (2013).
7. I. Buttinoni, J. Cha, W.-H. Lin, S. Job, C. Daraio, L. Isa, Direct observation of impact propagation and absorption in dense colloidal monolayers. *Proc. Natl. Acad. Sci. U.S.A.* **114**, 12150–12155 (2017).
8. P. Grasland-Mongrain, A. Zorgani, S. Nakagawa, S. Bernard, L. G. Paim, G. Fitzharris, S. Catheline, G. Cloutier, Ultrafast imaging of cell elasticity with optical microelastography. *Proc. Natl. Acad. Sci. U.S.A.* **115**, 861–866 (2018).

9. R. Mallet, On the dynamics of earthquakes; being an attempt to reduce their observed phenomena to the known laws of wave motion in solids and fluids. *Trans. R. Irish Acad.* **21**, 51–105 (1846).
10. D. T. N. Chen, Q. Wen, P. A. Janmey, J. C. Crocker, A. G. Yodh, Rheology of soft materials. *Annu. Rev. Condens. Matter Phys.* **1**, 301–322 (2010).
11. L. Bocquet, A. Colin, A. Ajdari, Kinetic theory of plastic flow in soft glassy materials. *Phys. Rev. Lett.* **103**, 036001 (2009).
12. J. Goyon, A. Colin, G. Ovarlez, A. Ajdari, L. Bocquet, Spatial cooperativity in soft glassy flows. *Nature* **454**, 84–87 (2008).
13. D. E. Discher, P. Janmey, Y.-L. Wang, Tissue cells feel and respond to the stiffness of their substrate. *Science* **310**, 1139–1143 (2005).
14. J. T. B. Overvelde, T. Kloek, J. J. A. D'haen, K. Bertoldi, Amplifying the response of soft actuators by harnessing snap-through instabilities. *Proc. Natl. Acad. Sci. U.S.A.* **112**, 10863–10868 (2015).
15. B. A. Auld, *Acoustic Fields and Waves in Solids* (Krieger Publishing Company, 1973).
16. J. R. Raney, N. Nadkarnic, C. Daraio, D. M. Kochmann, J. A. Lewis, K. Bertoldi, Stable propagation of mechanical signals in soft media using stored elastic energy. *Proc. Natl. Acad. Sci. U.S.A.* **113**, 9722–9727 (2016).
17. We estimate the Reynolds number as $Re \approx \rho_L \omega A_0 a/\eta$, with ρ_L and η the density and viscosity of the solvent and ωA_0 giving the maximum velocity of the probe.
18. L. D. Landau, E. M. Lifshitz, *Theory of Elasticity (Volume 7 of A Course of Theoretical Physics*) (Pergamon Press, 1970).
19. G. N. Greaves, A. L. Greer, R. S. Lakes, T. Rouxel, Poisson's ratio and modern materials. *Nat. Mater.* **10**, 823–837 (2011).
20. P. H. Mott, C. M. Roland, Limits to poissons ratio in isotropic materials. *Phys. Rev. B* **80**, 132104 (2009).
21. D. Boal, *Mechanics of the Cell* (Cambridge Univ. Press, ed. 2, 2012).
22. C. L. Klix, F. Ebert, F. Weysser, M. Fuchs, G. Maret, P. Keim, Glass elasticity from particle trajectories. *Phys. Rev. Lett.* **109**, 178301 (2012).
23. S. Vivek, C. P. Kelleher, P. M. Chaikin, E. R. Weeks, Long-wavelength fluctuations and the glass transition in two dimensions and three dimensions. *Proc. Natl. Acad. Sci. U.S.A.* **114**, 1850–1855 (2017).
24. G. L. Hunter, E. R. Weeks, The physics of the colloidal glass transition. *Rep. Prog. Phys.* **75**, 066501 (2012).
25. A. Zaccone, E. Scossa-Romano, Approximate analytical description of the nonaffine response of amorphous solids. *Phys. Rev. B* **83**, 184205 (2011).
26. T. G. Mason, D. A. Weitz, Optical measurements of frequency-dependent linear viscoelastic moduli of complex fluids. *Phys. Rev. Lett.* **74**, 1250–1253 (1995).
27. E. M. Furst, Applications of laser tweezers in complex fluid rheology. *Curr. Opin. Coll. Int. Sci.* **10**, 79–86 (2005).
28. J. C. Crocker, M. T. Valentine, E. R. Weeks, T. Gisler, P. D. Kaplan, A. G. Yodh, D. A. Weitz, Two-point microrheology of inhomogeneous soft materials. *Phys. Rev. Lett.* **85**, 888–891 (2000).
29. D. Allan, C. van der Wel, N. Keim, T. A. Caswell, D. Wieker, R. Verweij, C. Reid, Thierry, L. Grueter, K. Ramos, apiszcz, zoeith, R. W. Perry, F. Boulogne, P. Sinha, pfigliozzi, N. Bruot, L. Uieda, J. Katins, H. Mary, A. Ahmadia, soft-matter/trackpy: Trackpy v0.4 (2018).
30. J. C. Crocker, D. G. Grier, Methods of digital video microscopy for colloidal studies. *J. Coll. Int. Sci.* **179**, 298–310 (1996).
31. F. Gittes, C. F. Schmidt, Interference model for back-focal-plane displacement detection in optical tweezers. *Opt. Lett.* **23**, 7–9 (1998).
32. M. Atakhorrami, K. M. Addas, C. F. Schmidt, Twin optical traps for two-particle cross-correlation measurements: Eliminating cross-talk. *Rev. Sci. Instrum.* **79**, 043103 (2008).
33. Y. von Hansen, A. Mehlich, B. Pelz, M. Rief, R. R. Netz, Auto- and cross-power spectral analysis of dual trap optical tweezer experiments using Bayesian inference. *Rev. Sci. Instrum.* **83**, 095116 (2012).
34. K. Berg-Sørensen, H. Flyvbjerg, Power spectrum analysis for optical tweezers. *Rev. Sci. Instrum.* **75**, 594 (2004).
35. P. M. Hansen, I. M. Tolic-Nørrelykke, H. Flyvbjerg, K. Berg-Sørensen, tweezercalib 2.1: Faster version of Matlab package for precise calibration of optical tweezers. *Comput. Phys. Commun.* **175**, 572–573 (2006).
36. E.-L. Florin, A. Pralle, E. H. K. Stelzer, J. K. H. Hörber, Photonic force microscope calibration by thermal noise analysis. *Appl. Phys.* **66**, S75–S78 (1998).
37. iMatix Corporation (2015); http://zeromq.org/.
38. B. E. A. Saleh, M. C. Teich, B. E. Saleh, *Fundamentals of Photonics* (Wiley New York, 1991), vol. 22.
39. B. Kavčič, D. Babić, N. Osterman, B. Podobnik, I. Poberaj, Rapid prototyping system with sub-micrometer resolution for microfluidic applications. *Microsyst. Technol.* **18**, 191–198 (2011).

Acknowledgments

Funding: This work is part of the Industrial Partnership Program Hybrid Soft Materials that is carried out under an agreement between Unilever Research and Development B.V. and the Netherlands Organisation for Scientific Research (NWO). J.v.d.G. acknowledges the European Research Council for financial support (ERC Consolidator grant Softbreak). The work of J.S. is part of the VIDI research program (no. 723.016.001) of NWO. **Author contributions:** J.M.v.D. and J.S. conceived the experiments. J.M.v.D., R.W., and R.F. constructed and programmed the optical tweezer instrument. J.M.v.D. and R.H. developed the real-time distributed particle tracking protocol. J.M.v.D. performed the experiments and data analysis. J.v.d.G. developed the wave propagation theory. J.M.v.D., J.v.d.G., A.Z., and J.S. discussed the data interpretation and cowrote the manuscript. **Competing interests:** The authors declare that they have no competing interests. **Data and materials availability:** All data needed to evaluate the conclusions in this paper are present in the paper and/or the Supplementary Materials. Additional data related to this paper may be requested from the authors.

Submitted 20 December 2019
Accepted 19 June 2020
Published 11 September 2020
10.1126/sciadv.aba6601

Citation: J. M. van Doorn, R. Higler, R. Wegh, R. Fokkink, A. Zaccone, J. Sprakel, J. van der Gucht, Propagation and attenuation of mechanical signals in ultrasoft 2D solids. *Sci. Adv.* **6**, eaba6601 (2020).